NMR and spin relaxation in systems with magnetic nanoparticles: effects of size and molecular motion

2009 J. Phys.: Condens. Matter 21 255301

(http://iopscience.iop.org/0953-8984/21/25/255301)

J. Phys.: Condens. Matter **21** (2009) 255301 (7pp) doi:10.1088/0953-8984/21/25/255301

NMR and spin relaxation in systems with magnetic nanoparticles: effects of size and molecular motion

N Noginova[1], T Weaver[1], A Andreyev[2], A Radocea[3] and V A Atsarkin[4]

[1] Center for Materials Research, Norfolk State University, Norfolk, VA, 23504, USA
[2] Virginia Tech, Blacksburg, 24063, VA, USA
[3] Cornell University, Ithaca, 14853, NY, USA
[4] Kotelnikov Institute of Radio Engineering and Electronics RAS, 125009, Moscow, Russia

Received 2 March 2009, in final form 8 May 2009
Published 1 June 2009
Online at stacks.iop.org/JPhysCM/21/255301

Abstract

To better understand the specifics of nuclear magnetic resonance and spin relaxation in systems with magnetic nanoparticles and test the limits of the outer sphere model for the diffusion-related relaxation, iron oxide nanoparticle suspensions are studied in dependence on the particle concentration and size (5–40 nm). The model is modified to account for aggregation of the particles into clusters with an enlarged effective radius. For liquid suspensions containing small particles or clusters, both the longitudinal and transverse spin relaxation rates, T_1^{-1} and T_2^{-1}, correspond well to the theory, which predicts passing of T_1^{-1} through a maximum and monotonic increase in T_2^{-1} with increasing particle size. For the largest particle sizes, as well as in the case of strong aggregation, the relaxation rates are significantly lower than theoretical predictions. An abrupt change in both the relaxation rates is observed in a narrow temperature range around the melting point of paraffin wax doped with magnetic nanoparticles. The applicability of fast-motion and fast-diffusion approximations is discussed for large effective sizes and limiting molecular motion cases.

(Some figures in this article are in colour only in the electronic version)

1. Introduction

Magnetic nanoparticles (NPs) are promising for many applications in technology, biology and medicine, including medical hyperthermia, drug delivery, MRI contrast agents etc. Due to the high magnetic moment of a single nanoparticle, even a small number of the particles results in significant changes in magnetic resonance spectra and spin relaxation rates of surrounding nuclei [1–4].

In [4], the effect of the γ-Fe_2O_3 (maghemite) nanoparticles on NMR properties was studied in various matrices, and found to be very different in liquid and solid systems. In toluene and water solutions, adding NPs resulted in the homogeneous broadening of the ^{1}H NMR spectra and substantial increase in the nuclear relaxation rates, whereas the inhomogeneous NMR broadening without any effect on nuclear relaxation has been observed in solid suspensions. These results were explained on the assumption that the nuclear spin relaxation is caused by time-dependent variations of the local magnetic fields seen by the nuclei during diffusional motion in a spatial nonuniform field created by NPs. The mechanism related to the thermal fluctuations of the NP magnetic moments, μ, was shown to make a much lower contribution due to the almost total NP polarization in the external magnetic field $B = 7$ T [4].

The self-diffusion mechanism of the nuclear spin relaxation in liquid solutions with magnetic particles is commonly described [3] using the standard outer sphere model, which was originally developed for paramagnetic impurities [5, 6]. To fit the experimental data obtained in [4], the model was modified to take into account the formation of small aggregates. This approach was verified, however, only on suspensions containing NPs with the relatively small diameter $d = 5$ nm. It would be of interest to test this approach on nanoparticle samples of various sizes.

Table 1. The parameters of the samples and ^{1}H spin relaxation rates (room temperature, $B = 7$ T).

Sample	$r = d/2$ (nm)	M_g (Oe g^{-1})	Concentration, (mg ml^{-1})	T_1^{-1} (s^{-1})	T_2^{-1} (s^{-1})	T_1/T_2	R (nm)
Sample 5	2.5	4	3.6	0.47	11.3	24	4.9
			10.8	1.1	56	52	6
			17.7	1.6	160	96	7
Sample 10A	4.5	25	10.8	62	750	12.1	3.81
			21.6	95	1 130	11.9	3.67
Sample 10B	5	11	3.6	0.22	1 010	4 700	20
			18	25	1 570	62.8	6.3
Sample 20	10	20	3.6	0.9	4 400	4 790	19.5
			10.8	4.0	15 700	3 800	18.4
			21.6	11.1	31 400	2 840	17
Sample 40	20	18	10.8	0.15	2 330	15 000	27.3
			21.6	0.2	4 150	20 800	30

Another problem to be explored relates to the limits of the fast-motion approximation, which constitutes the basis of the standard theory [3, 5, 6]. The most important is the diffusional correlation time τ_D, which is assumed to be of the order of R^2/D, where D is the self-diffusion constant and R is the characteristic parameter related to the radius of the magnetic impurity. The fast-motion approximation implies that τ_D is sufficiently short as compared with other characteristic times of the system (this point will be considered in more detail in section 4). This requirement is commonly fulfilled in liquids doped with paramagnetic ions or molecular complexes characterized by relatively small R and μ values. However, if the molecular motion is too slow (as it is for solids), or the effective particle size or magnetic moment are too large (as it may be for NPs even in liquid suspensions), the basic assumptions of the model would be broken.

This question is important for applications as well: how the relaxation rates T_1^{-1} and T_2^{-1} depend on the particle size, if the same amount of NPs by weight is added to the system; and at which size the particles would produce the largest effect on the spectra and relaxation rates.

The goal of this study is to obtain more information on NMR and spin relaxation processes in the systems with magnetic nanoparticles, and test the limits of the existing model.

2. Experimental details

In the main series of the experiments we have studied the NMR spectra and spin relaxation kinetics in chloroform suspensions of Fe_3O_4 (magnetite) nanoparticles with the diameter of 5, 10 (several different lots), 20 and 40 nm. The measurements were performed at room temperature. The dense chloroform suspensions of the particles (with oleic acid as a surfactant) were purchased from Ocean NanoTech. According to TEM characterization, the samples have a narrow size distribution of ± 0.1 nm. Static magnetic properties were characterized with a SQUID magnetometer. Saturated magnetization values (M_g) are shown in table 1 per gram of the corresponding dry powder. They are substantially lower than the table value for the bulk magnetite, $M_g = 86$ Oe g^{-1} [7]. The decreased value is rather typical of nanoscale objects and could be related to the quality of the samples, presence of nonmagnetic phases and surface related effects [8]. To prepare experimental samples, the dense ferrofluid suspensions were diluted in the chloroform in various concentrations and sonicated.

The experimental data reported here were obtained with suspensions which were stable enough and did not deteriorate with time. The NMR spectra and kinetics in these samples showed practically no changes in the period up to several days. Note, however, that some suspensions prepared from different lots demonstrated slight changes in coloration and transparency, as well in the NMR parameters, several hours after the preparation. The data on the unstable suspensions are not included.

Supplementary experiments aimed at revealing the difference between the fast- and slow-motion limits were performed on suspensions of NPs in paraffin wax (Aldrich), in the vicinity of the melting point (50 °C). Surface modified particles of γ-Fe_2O_3 (maghemite) with the diameter of 5 nm were used. The details of the fabrication and characterization of the solvent-free γ-Fe_2O_3 ferrofluid can be found in [9]. To prepare experimental samples, the mixture of paraffin and NPs (with the concentration of NPs of about ~2 wt%) was heated to ~70 °C and sonicated.

The ^{1}H NMR spectra were studied using a Bruker Avance 300 NMR spectrometer working in the magnetic field $B = 7$ T at the frequency of $\omega_I/2\pi = 300$ MHz. The duration of the $\pi/2$ pulse was 6 μs. The spin–lattice relaxation time T_1 was determined from the magnetization kinetics using the standard inversion recovery technique. The transverse relaxation time T_2 was measured from the free induction decay or estimated from the line width (no spin echo was observed in liquid NP suspensions).

3. Experimental results

3.1. Effect of the particle size and aggregation

The liquid NP suspensions demonstrate significantly broadened NMR spectra and higher spin–lattice relaxation rates as compared with the pure solvent. An example in figure 1

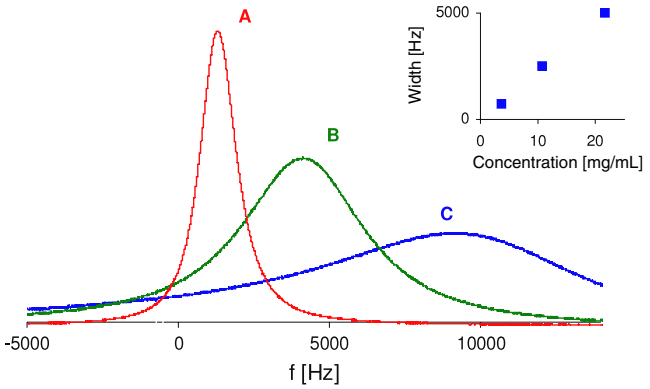

Figure 1. Proton NMR spectra in chloroform solutions with 20 nm Fe_3O_4 nanoparticles with the concentration 3.6 (trace A), 10.8 (B), and 21.6 mg ml^{-1} (C). The zero on the frequency axis corresponds to chloroform without NPs. Inset: the half-width of the line estimated from the fitting with the Lorentzian function.

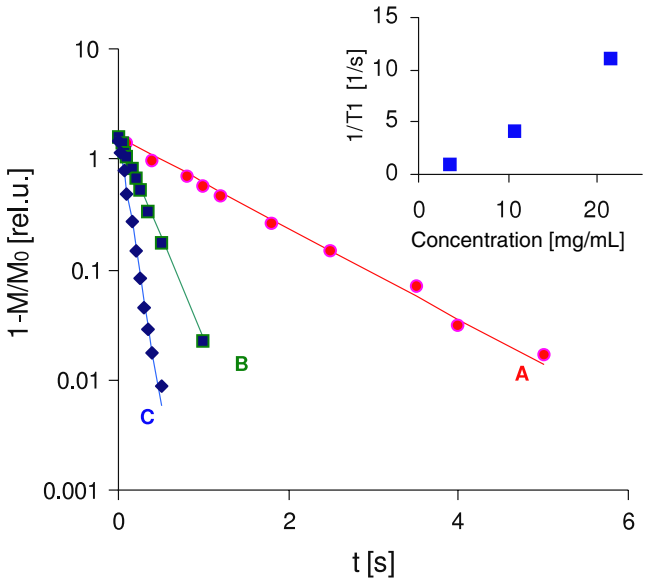

Figure 2. Magnetization recovery kinetics in the chloroform solutions with 20 nm size Fe_3O_4 nanoparticles with the same concentrations (A, B, C) as in figure 1. Inset: NP contribution to the relaxation rate, $1/T_1$.

demonstrates the ^{1}H spectra for the chloroform solution containing 20 nm size particles with the concentrations related as 1:3:6, where unity corresponds to the ferrite concentration (C) of 3.6 mg ml^{-1}. The spectral width (see the inset) is approximately proportional to the concentration. In all the samples studied in this experiment, the spectrum can be described with a single Lorentzian line, indicating homogeneous character of broadening in the liquid samples. This was confirmed by the absence of the spin echo signals after the free induction decay (see also the results of [4]). The shift of the spectral line is observed as well. The origin of the shift can be ascribed to both chemical and demagnetization effects [10].

The kinetics of the spin–lattice relaxation for the same set is shown in figure 2. The magnetization recovery can be described with a single exponential function. The NP related contribution to the relaxation rate is estimated as $1/T_1 = 1/T_1^{\rm exp} - 1/T_1^{\rm ch}$, where $T_1^{\rm exp}$ is the relaxation time measured for the suspension with the NPs, and $T_1^{\rm ch}$ of 30 s is the relaxation time for the pure chloroform. As shown in the inset, the NP contribution grows approximately linearly with the increase in the particle concentration above 3.6 mg ml^{-1}, similar to observations of [4].

The other samples studied demonstrate similar behavior; however, broadening and growth of the relaxation rates are not always strictly proportional to the concentration.

The results of the experiments are summarized in table 1.

The relaxation rates, normalized to the NP concentration of 10 mg ml^{-1} as

$$(T_{1,2,N})^{-1} = 10(T_{1,2})^{-1}/C$$

(in the assumption of the linear dependence on C), are plotted in dependence on the nominal radius of the particle, $r = d/2$, in figure 3.

Although the data are very scattered, some general tendencies can be seen, such as the decrease of the longitudinal relaxation rate and increase of the transverse relaxation rate with the increase in the particle size. A more detailed analysis of the data taking into account the different sample magnetization and cluster formation will be discussed later.

3.2. Supplementary experiments: the effects of NPs during the solid–liquid phase transformation

As discussed earlier, the presence of NPs in the medium causes the spectral broadening for both liquid and solid matrices, while the effects on the spin relaxation rates are completely different for these two kinds of systems. A significant acceleration in the relaxation was observed for the liquid suspensions, and practically no effect was detected for solids. To observe such a different behavior and monitor dramatic changes in nuclear spin relaxation in the same matrix, we performed the measurements in the vicinity of the liquid-to-solid phase transition. In our experiments, we studied the spin–lattice relaxation of protons in paraffin containing γ-Fe_2O_3 magnetic nanoparticles in the temperature range of the paraffin melting (∼50 °C). For comparison, we also measured the spin relaxation kinetics for the pure paraffin below and above the phase transition (at 25 °C and 60 °C, respectively), in both cases obtaining similar values for the relaxation time, $T_1^0 = (1.35 \pm 0.05)$ s.

The results of the measurements in the system with NPs are shown in figure 4. Below the transition, at 45 °C, the spin relaxation is slow with a rate similar to that observed in the pure paraffin. At elevated temperatures, another, faster component appears. It becomes more and more pronounced with the increase in temperature.

At the temperatures well above the transition only the fast component exists in the system with NPs, in sharp contrast with the slow relaxation in the pure paraffin. The experimental data presented in figure 4 could be fitted with the sum of two exponential functions

$$A_1 \exp(-t/T_{1s}) + A_2 \exp(-t/T_{1f}),$$

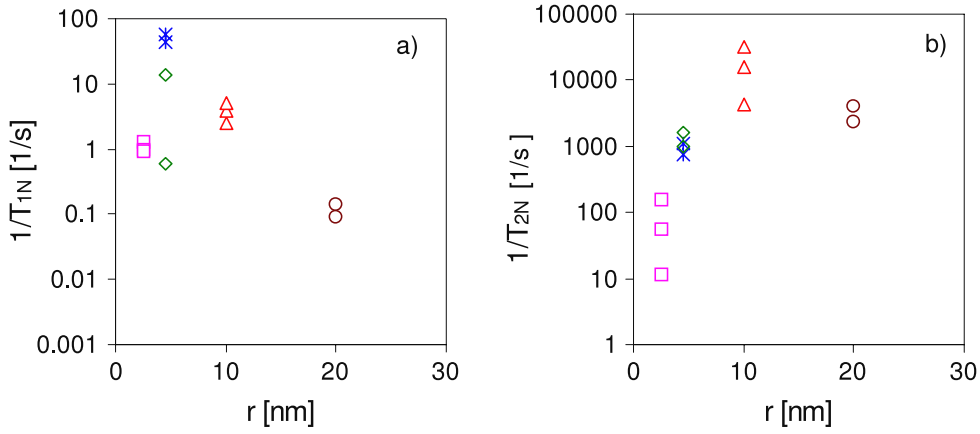

Figure 3. The proton relaxation rates in the suspensions with NPs (normalized per 10 mg ml^{-1}) in dependence on the particle size. Different symbols correspond to different sets of the samples. Squares, sample 5; stars, sample 10A; diamonds, sample 10B; triangles, sample 20; circles, sample 40.

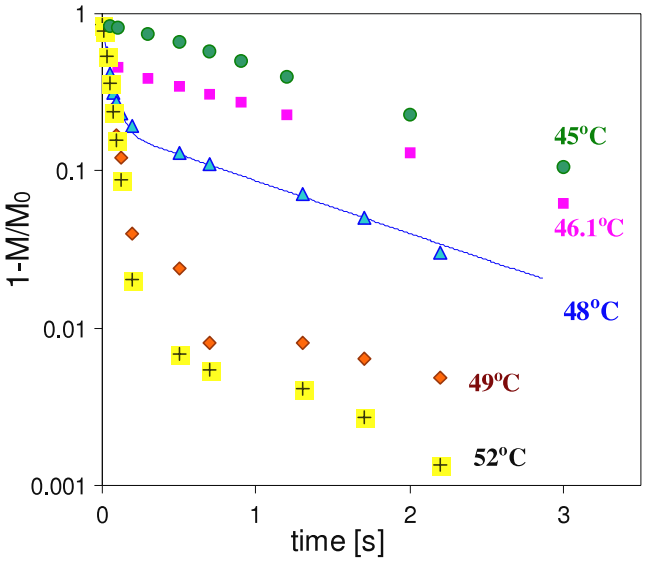

Figure 4. Magnetization recovery kinetics in the NP/paraffin suspension. Temperatures are indicated in the figure. The solid trace is the fitting with the sum of two exponentials.

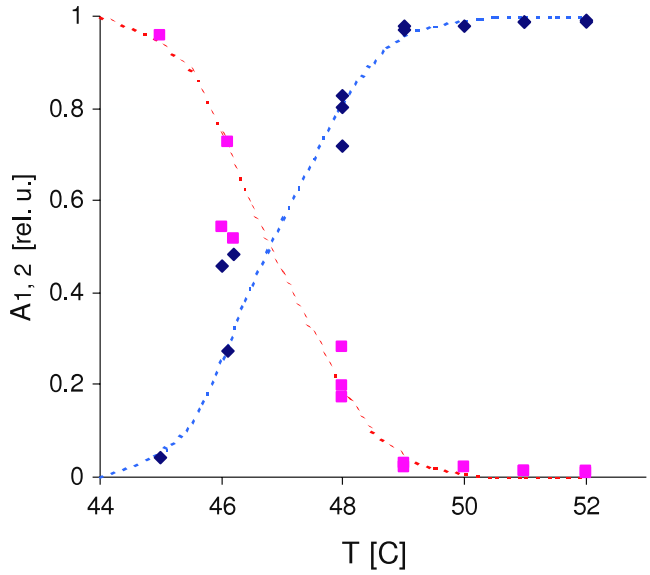

Figure 5. The amplitudes of the fast (diamonds) and slow (squares) components in the relaxation kinetics in the NP/paraffin suspension; the dotted traces are guides for the eyes.

where $T_{1s} = (1.40 \pm 0.05)$ s and $T_{1f} = (0.051 \pm 0.005)$ s. The relative weight of the fast and slow components in dependence on temperature is shown in figure 5. As one can see, the radical change in the relaxation rate takes place in the interval 45–49 °C, just below the melting temperature of paraffin, 50 °C.

4. Discussion

Let us first discuss the effect of the particle size on the nuclear relaxation rates in the chloroform suspensions. The standard diffusion-related mechanism of the nuclear relaxation in a medium containing magnetic impurities (the outer sphere model) predicts [3]

$$\frac{1}{T_1} = \frac{32\pi}{135}\gamma_I^2 \frac{n}{RD}[3J^A(\sqrt{2\omega_I \tau_D})\langle\mu_z\rangle^2] \qquad (1)$$

$$\frac{1}{T_2} = \frac{32\pi}{135}\gamma_I^2 \frac{n}{RD}\left[\frac{3}{2}J^A(\sqrt{2\omega_I \tau_D}) + 2J^A(0)\right]\langle\mu_z\rangle^2. \qquad (2)$$

Here γ_I is the gyromagnetic ratio of the proton, D is the self-diffusion constant of the solvent (for chloroform at 300 K, $D = 2.35 \times 10^{-5}$ cm^2 s^{-1}), n is the number of particles per unit volume, μ is the magnetic moment, R is the effective radius associated with a magnetic nanoparticle, $\tau_D = R^2/D$, and $J^A(z)$ is the spectral density of the correlation function related to molecular diffusion in the inhomogeneous local magnetic field produced by the magnetic particles,

$$J^A(z) = \frac{1 + 5z/8 + z^2/8}{1 + z + z^2/2 + z^3/6 + z^4/81 + z^5/81 + z^6/648}. \qquad (3)$$

The terms accounting for the fluctuations of the particle magnetic moment are omitted because of nearly total NP polarization in the field $B = 7$ T.

In our experiments we use samples with different magnetizations and radii. To compare them to each other and to the model, let us rewrite the formulae (1) and (2) in the normalized form, which enables one to discuss the data relating to the fixed concentration of the magnetic material and thus to account for the cluster formation. To use the quantities determined directly from the SQUID measurements, we express n and $\langle\mu\rangle$ as

$$n = C/m; \qquad \langle\mu\rangle = M_g m,$$

where m is the net mass of the ferrite in a magnetic object which can be now either the single particle or a cluster consisting of several particles coupled by magnetic dipole–dipole interaction. Such a sort of aggregation is well known in magnetic fluids, especially under conditions of strong polarization in the external magnetic field (see, for example, [11]). Further, one has

$$m = V\rho/\alpha$$

where V is the particle (or cluster) volume, ρ is the ferrite density, and $\alpha \geqslant 1$ is the coefficient introduced to take into account a nonmagnetic part of the cluster. Assuming a spherical shape of the cluster (so $V = 4\pi R^3/3$) and substituting the foregoing expressions in equations (1) and (2), one gets for the normalized relaxation rates

$$(T_1^{-1})_{\text{norm}} \equiv \frac{T_1^{-1}}{CM_g^2} = \frac{4\pi}{3}\frac{32\pi}{135D}\gamma_I^2\frac{\rho R^2}{\alpha}3J^A\left(R\sqrt{\frac{2\omega_I}{D}}\right) \quad (4)$$

$$(T_2^{-1})_{\text{norm}} \equiv \frac{T_2^{-1}}{CM_g^2} = \frac{4\pi}{3}\frac{32\pi}{135D}\gamma_I^2\frac{\rho R^2}{\alpha} \times \left[\frac{3}{2}J^A\left(R\sqrt{\frac{2\omega_I}{D}}\right) + 2J^A(0)\right]. \quad (5)$$

Note that, according to equations (4) and (5), the ratio T_1/T_2 does not depend on the concentration and weight magnetization but is determined solely by the radius R as

$$\frac{T_1}{T_2} = \frac{\frac{3}{2}J^A(\sqrt{2\omega_I\tau_D}) + 2J^A(0)}{3J^A(\sqrt{2\omega_I\tau_D})} \approx \frac{2}{3J^A\left(R\sqrt{\frac{2\omega_I}{D}}\right)}. \quad (6)$$

The second (approximate) equality is due to the fact that $J^A(0) = 1$ is much higher than $J^A(\sqrt{2\omega_I\tau_D})$, which ranges within 10^{-5}–10^{-2} in our experimental conditions. Commonly, R is considered to be of about a nanoparticle size; however, it may be significantly larger due to the aggregation of nanoparticles. The model predicts monotonic growth of T_1/T_2 with the increase of the effective radius; see figure 6 (solid trace).

Let us add our experimental data to this plot first as a function of a nominal particle radius r (open symbols). For each data point let us find the effective radius R at which the experimental value of T_1/T_2 would correspond to the model, as illustrated in figure 6.

The values of the effective radius obtained this way are shown in the last column of the table 1. As one can see, in some cases (i.e. for sample 10A) the effective value of R is close to the corresponding size of the particle. In other cases, however, it significantly exceeds this (as for sample 10B). This can be ascribed to the formation of large clusters.

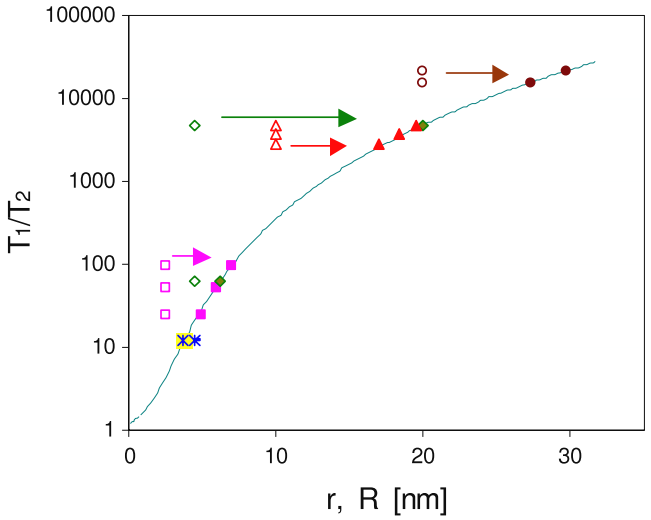

Figure 6. The ratio T_1/T_2 in dependence on the real particle radius r (the same open symbols as in figure 3) and effective radius R (filled symbols of the same shapes). The solid trace is equation (6).

Figure 7 demonstrates the predictions of equations (4) and (5) for $\alpha = 1$ and our experimental data plotted versus the effective radius estimated from figure 6. According to equation (4), the longitudinal relaxation rate passes though a maximum at $R \sim 2.5$ nm and then decreases with the increase in the effective radius. In contrast, the transverse relaxation rate grows monotonically with the particle size.

As one can see, the normalized experimental data plotted versus the effective radius are consistent with the theoretical predictions in a wide range up to $R = 20$ nm. The model works in both cases, when the effective radius is close to the particle size (individual particles) or exceeds this considerably (clusters). Estimating the number of particles in a cluster as

$$N = \frac{1}{\alpha}\left(\frac{R}{r}\right)^3, \quad (7)$$

one obtains N as from 8 to 20 in the suspensions of sample 5, of about 3 for sample 20, up to 60 for sample 10B and $N = 1$ (no aggregation) in sample 10A. The cause of the observed difference in the aggregation ability is not clear yet; perhaps this is related to the specifics of the surfactant behavior.

For $R > 20$ nm, both T_1^{-1} and T_2^{-1} start to systematically deviate from the predictions of the model. The discrepancy becomes very pronounced for larger R: at 30 nm, the experimental data are lower than the theoretical values by more than the order of magnitude. One way to explain this disagreement is to adjust α, supposing progressive increase of the nonmagnetic volume in the aggregates. However, at large enough R, this becomes unrealistic, leading to $\alpha \sim 30$ for sample 40.

Another way is to discuss the limitations of the theory. Among the main assumptions of the model are the following. (1) Equations (1) and (2) are based on the general theory of spin relaxation caused by fast molecular motion [12]. In this

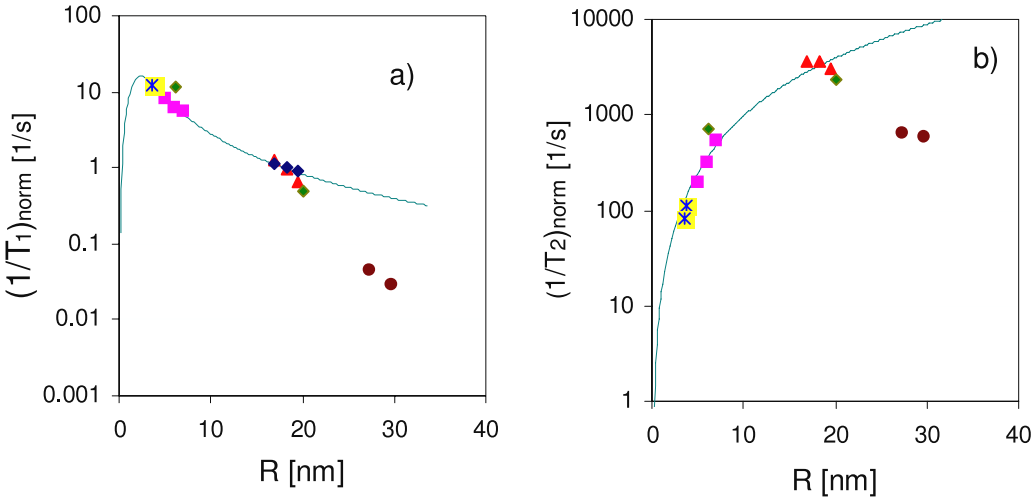

Figure 7. The normalized relaxation rates versus the effective radius. The symbols are the same as in figure 6.

approach, the relaxation times (T_1, T_2) are assumed to be much longer than the correlation times of the fluctuations which induce the relaxation process. For the longitudinal relaxation, this assumption reduces to the predominance of the nuclear Larmor frequency $\omega_I = \gamma_I B$ over the frequency shift due to the local field created by the NPs. In our case, this is equivalent to the inequality $B \gg \mu/R^3 = 4\pi\rho M_g/3$; this certainly holds for $B = 7$ T. For the transverse relaxation (T_2), however, the situation is more complicated. Now, the same basic assumption suggests that the average frequency $1/\tau_D$ of the local field fluctuations exceeds the fluctuation magnitude expressed in the frequency units. Considering diffusional motion of a molecule at the minimum distance R from an NP, one has

$$\tau_D^{-1} = D/R^2 > \gamma_I \mu/R^3, \tag{8}$$

or, substituting for $\mu = (4\pi/3)R^3\rho M_g$,

$$R < [3D/(4\pi\gamma_I \rho M_g)]^{1/2}. \tag{8a}$$

For our samples, this inequality breaks near $R \sim 15$ nm and, hence, excludes applicability of equations (2), (5) and (6) for $R > 20$ nm, where the experimental points in figure 7 deviate from the theory. In this range, the molecular motion is not fast enough to average the inhomogeneity of the local fields, and the situation is shifted toward the solid-state limit.

(2) Even if the above-mentioned condition is fulfilled, another problem can arise for a relatively large NP radius and a low concentration. In the frames of the outer sphere model [5], the self-diffusion is assumed to be fast enough to provide multiple passages of a molecule between the magnetic particles before the relaxation occurs. This leads to the condition

$$R_0^2/D \ll T_1(R),\ T_2(R) \tag{9}$$

where $R_0 = R/(C/\rho)^{1/3}$ is the radius of the 'sphere of influence' of a magnetic particle and $T_1(R)$, $T_2(R)$ are the relaxation rates of a molecule at the minimum distance of the NP. The inequality (9) is inevitably broken at low enough concentration of the magnetic particles. In such a case, the fast-diffusion process assumed in equations (1) and (2) is transformed into the diffusion limited relaxation which is beyond the applicability of the standard outer sphere model. The analysis shows that the fast-diffusion condition, equation (9), can be violated for our largest particles, such as sample 40. (At a given weight concentration C, the number of NPs in unit volume is inversely proportional to R^3.) Currently there is no rigorous theory for this situation. Qualitatively, it is clear that nuclear relaxation should be retarded as compared with equations (1) and (2), as occurs in the case of the limited spin diffusion in solids with paramagnetic impurities [13]. This prediction agrees with our experimental data; see figure 7.

The data obtained on the paraffin wax, figures 4 and 5, are no more than a clear illustration of stepping outside the frames of the fast-motion and fast-diffusion approximations. In this case, the liquid-to-solid transition results in a very steep transfer to the slow-motion limit. In the transition range, a complex kinetics could be expected. However, as seen from figure 4, only two relaxation rates are revealed, corresponding to the liquid and solid phases, without an intermediate state. Gradual change in the magnitudes of the fast and slow exponentials (figure 5) suggests co-existence of both phases in a narrow temperature range (45–49 °C). Thus, additional experiments with viscous liquids or gels should be performed to study the boundary region in more detail.

5. Conclusion

Our results obtained in liquid suspensions of the iron oxide nanoparticles with various sizes demonstrate that for small enough nanoparticles or clusters ($R \leqslant 20$ nm) the nuclear spin relaxation can be satisfactory described with the outer sphere model modified to account for the possible cluster formation. This approach enables one to reveal clusters in magnetic suspensions, and estimate the cluster size.

For larger particle sizes or in the case of strong aggregation ($R > 20$ nm), the experimental data deviate from the predictions and demonstrate significantly decreased relaxation rates. A steep drop in the relaxation rate T_1^{-1} is observed as

well with the slowdown of molecular motion during liquid-to-solid transition in the paraffin wax. This behavior can be explained by limitations of the model. In particular, the fast-motion and fast-diffusion approximations cease to be valid in these cases. Further experimental work, as well as development of the theory beyond the fast-motion approximation and under conditions of limited molecular diffusion, is absolutely necessary.

Acknowledgments

The work was partly supported by National Science Foundation (NSF) PREM grant DMR-0611430. One of the authors (VAA) acknowledges support of the Russian Foundation for Basic Research (grant 08-02-00040) and the Russian Academy of Sciences (Program P03-2-24).

References

[1] Roch A, Gillis P, Ouakssim A and Miller R N 1999 *J. Magn. Magn. Mater.* **201** 77–9
[2] Bautista M C, Bomati-Miguel O, Zhao X, Morales M P, Gonzáles-Carreño T, Pérez de Alejo R, Ruiz-Cabello J and Veintemillas-Verdaguer S 2004 *Nanotechnology* **15** S154–9
[3] Roch A, Muller R N and Gillis P 1999 *J. Chem. Phys.* **110** 5403–5411
[4] Noginova N, Weaver T, King M, Bourlinos A B, Giannelis E P and Atsarkin V A 2007 *J. Phys.: Condens. Matter* **19** 076210
[5] Freed J U 1978 *J. Chem. Phys.* **68** 4034
[6] Toth E, Helm L and Merbach A E 2002 Relaxivity of MRI Contrast Agents *Topics in Current Chemistry* vol 221 (Berlin: Springer) pp 61–101
[7] Rosensweig R E 2002 *J. Magn. Magn. Mater.* **252** 370
[8] Novakova A A, Lanchinskaya V Yu, Volkov A V, Gendler T S, Kiseleva T Yu, Moskvina M A and Zezin S B 2003 *J. Magn. Magn. Mater.* **258/259** 354
[9] Bourlinos A B, Herrera R, Chalkias N, Jiang D D, Zhang Q, Archer L A and Giannelis E P 2005 *Adv. Mater.* **17** 234
[10] Lim A R, Kim C S and Choh S H 1992 *Bull. Magn. Reson.* **14** 240–5
[11] Horng H E, Hong C Y, Yang H C, Jang I J, Yang S Y, Wu J M, Lee S L and Kuo F C 1999 *J. Magn. Magn. Mater.* **201** 215
[12] Abragam A 1961 *The Principles of Nuclear Magnetism* (Oxford: Clarendon) Chapters 8, 10
[13] Khutsishvili G R 1969 *Sov. Phys.—Usp.* **11** 802